Targeted Delivery of Small Interfering RNA Using Reconstituted High-Density Lipoprotein Nanoparticles[1,2]

Mian M.K. Shahzad*,[†], Lingegowda S. Mangala[‡], Hee Dong Han*, Chunhua Lu*, Justin Bottsford-Miller*, Masato Nishimura*, Edna M. Mora[§],[¶], Jeong-Won Lee*,[#], Rebecca L. Stone*, Chad V. Pecot**, Duangmani Thanapprapasr*, Ju-Won Roh*, Puja Gaur[§], Maya P. Nair[††], Yun-Yong Park[‡‡], Nirupama Sabnis[††], Michael T. Deavers[§§], Ju-Seog Lee[‡‡], Lee M. Ellis[§],[¶¶], Gabriel Lopez-Berestein[¶¶],[##],***, Walter J. McConathy[†††], Laszlo Prokai[††], Andras G. Lacko[††] and Anil K. Sood*,[¶¶],***

*Department of Gynecologic Oncology, University of Texas MD Anderson Cancer Center, Houston, TX, USA; [†]Division of Gynecologic Oncology, Department of Obstetrics and Gynecology, University of Wisconsin School of Medicine and Public Health, Madison, WI, USA; [‡]Department of Radiation Biophysics, NASA Johnson Space Center, University of Space Research Association, Houston, TX, USA; [§]Department of Surgical Oncology, University of Texas MD Anderson Cancer Center, Houston, TX, USA; [¶]University of Puerto Rico Comprehensive Cancer Center and University of Puerto Rico School of Medicine, San Juan, Puerto Rico; [#]Department of Obstetrics and Gynecology, Samsung Medical Center, Seoul, South Korea; **Department of Cancer Medicine, University of Texas MD Anderson Cancer Center, Houston, TX, USA; [††]Department of Molecular Biology & Immunology, University of North Texas-HSC, Fort Worth, TX, USA; [‡‡]Department of Systems Biology, University of Texas MD Anderson Cancer Center, Houston, TX, USA; [§§]Department of Pathology, University of Texas MD Anderson Cancer Center, Houston, TX, USA; [¶¶]Department of Cancer Biology, University of Texas MD Anderson Cancer Center, Houston, TX, USA; [##]Department of Experimental Therapeutics, University of Texas MD Anderson Cancer Center, Houston, TX, USA; ***Center for RNA Interference and Non-coding RNA, University of Texas MD Anderson Cancer Center, Houston, TX, USA; [†††]Department of Internal Medicine, Texas Tech University–HSC, Fort Worth, TX, USA

Abstract

RNA interference holds tremendous potential as a therapeutic approach, especially in the treatment of malignant tumors. However, efficient and biocompatible delivery methods are needed for systemic delivery of small interfering RNA (siRNA). To maintain a high level of growth, tumor cells scavenge high-density lipoprotein (HDL) particles by overexpressing its receptor: scavenger receptor type B1 (SR-B1). In this study, we exploited this cellular characteristic to achieve efficient siRNA delivery and established a novel formulation of siRNA by incorporating it into reconstituted HDL (rHDL) nanoparticles. Here, we demonstrate that rHDL nanoparticles facilitate highly efficient systemic delivery of siRNA *in vivo*, mediated by the SR-B1. Moreover, in therapeutic proof-of-concept studies, these nanoparticles were effective in silencing the expression of two proteins that are key to cancer growth and metastasis (signal transducer and activator of transcription 3 and focal adhesion kinase) in orthotopic mouse models of ovarian and colorectal cancer. These data indicate that an rHDL nanoparticle is a novel and highly efficient siRNA carrier, and therefore, this novel technology could serve as the foundation for new cancer therapeutic approaches.

Neoplasia (2011) 13, 309–319

Introduction

RNA interference (RNAi) is being increasingly recognized as a potentially highly effective therapeutic approach [1–3]. This concept is rooted in the power of RNAi (e.g., small interfering RNA [siRNA]) to silence genes that are difficult to target with conventional approaches, such as antibodies or small molecule inhibitors. Although specific gene targeting by RNAi is indeed promising [4–6], efficient and biocompatible methods of *in vivo* siRNA delivery are needed to realize its full therapeutic potential. Although several transmembrane delivery methods have been reported using liposomes [7–9] or other nanoparticles [10–12], their therapeutic applications can be limited because of toxicities or other concerns. Therefore, new and more specific methods are needed for systemic delivery of siRNA.

Lipoproteins, especially high-density lipoprotein (HDL), are essential components of the lipid transport system. HDL plays a pivotal role in reverse cholesterol transport by promoting the return of excess cholesterol from peripheral cells to the liver for elimination (biliary excretion or use in enterohepatic cycle) [13]. Endogenously, HDL particles are completely biodegradable, and they have not been reported to elicit immunologic responses. In addition, because HDL particles are known to escape the reticuloendothelial system, they exhibit longer residence time in the circulation [14] than most drug formulations or other lipoproteins. The core contents of the circulating HDL particles are taken up through a receptor-mediated mechanism through scavenger receptor class B type 1 (SR-B1) that is primarily expressed in the liver [15,16] and most malignant cells [17]. On the basis of attractive features such as small size, shielded hydrophobic core, and the possibility of receptor mediated uptake by the targeted tumor cells [18,19], HDL nanoparticles are ideal drug carriers. Reconstituted HDL (rHDL) is the synthetic form of the circulating human HDL lipoprotein. The composition of rHDL nanoparticles includes phosphatidylcholine, apolipoprotein A-1, cholesterol, and cholesteryl esters [20] (Figure 1*A*). The rHDL nanoparticles are small with, an approximate diameter of 12 to 18 nm.

To develop targeted delivery approaches for siRNA [6,10,21], several tumor cell receptors have been examined. The SR-B1 receptor is expressed mainly in the liver and, to a lesser extent, in the adrenal glands or normal ovarian tissues [22–26]. However, SR-B1 expression in malignant cells is quite prominent. Increased uptake of HDL results in higher rates of tumor cell proliferation. For example, breast cancer cells increase uptake of cholesterol esters by increasing SR-B1 expression [14]. Thus, given the role of SR-B1 in HDL homing to tumor cells, we considered rHDL nanoparticles attractive for selective delivery of therapeutic payloads.

Use of siRNA for therapeutic silencing is particularly attractive for genes that are difficult to target with other approaches [27]. Signal transducer and activator of transcription 3 [STAT3] is known to mediate normal cellular response to a variety of cytokines and growth factors [28,29]. Activation of STAT3 results in key processes involved in malignant transformation and progression (e.g., cell proliferation, differentiation, and survival) [30]. Although STAT3 is activated in many solid tumors, it is known to be expressed in normal tissues and is involved in many normal cellular processes [28,29]. Therefore, using small molecule inhibitors or other nonspecific methods of targeting STAT3 could result in many unwanted adverse effects, and this warrants a more selective approach to limit toxicity. Similarly, focal adhesion kinase (FAK) is critical for tumor cell survival, migration, and invasion [31–34]. In ovarian cancer patients, FAK overexpression is linked to aggressive tumor features that contribute to poor overall survival [35]. For proof-of-concept, we demonstrate therapeutic efficacy by targeting both STAT3 and FAK by using the rHDL nanoparticle delivery method in ovarian and colorectal cancer models.

Materials and Methods

rHDL Nanoparticle Preparation and siRNA Incorporation

SiRNA was incorporated into rHDL nanoparticles [36] and stored at –20°C. Briefly, apolipoprotein A-I (Apo A-I), which is the major core protein in the rHDL particle, was isolated and purified using a plasmid vector for the production of protein [37]. Next, a mixture of lipids (cholesterol [C]/cholesteryl oleate [CE]/egg yolk phosphatidylcholine [PC], molar ratio of 1:5:1.3:115) was dried under a stream of nitrogen. Five micrograms of siRNA was preincubated with 25 μg of oligolysine
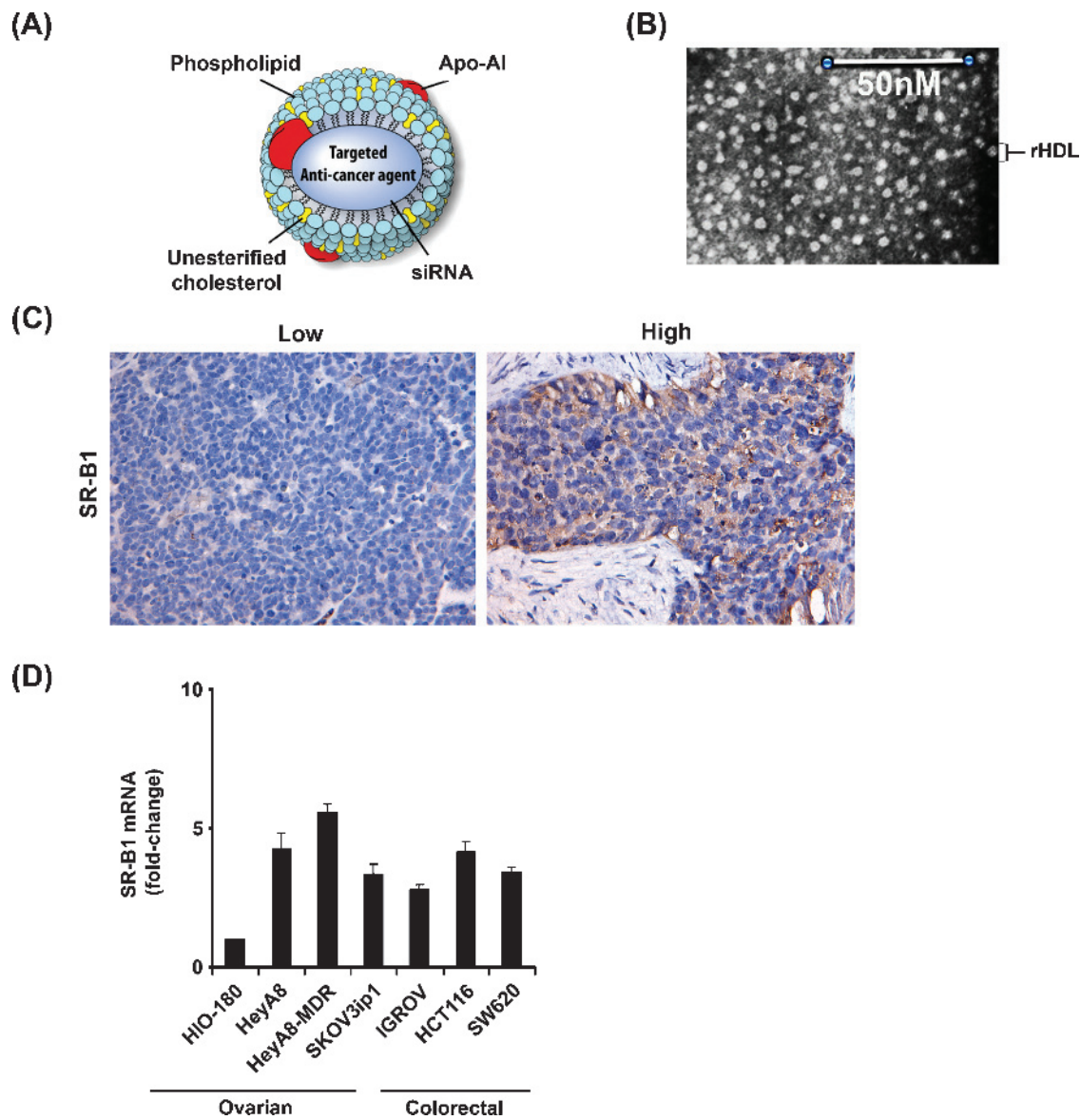
Figure 1. Characterization of rHDL nanoparticles. (A) Illustrations of rHDL nanoparticle composition. (B) Electron micrograph of rHDL nanoparticles containing control siRNA. (C) Expression of SR-B1 in human epithelial ovarian cancer (IHC). (D) mRNA expression of SR-B1 in ovarian and colorectal cancer cell lines.

(mean MWt, 500-2000) at 30°C, for 30 minutes, and then added to the lipid ingredients. The oligolysine/siRNA mixture was then combined with lipids and dispersed in 60 μl of DMSO and 1.4 ml of buffer (10 mM Tris, 0.1 M KCl, 1 mM EDTA pH 8.0). Sodium cholate, 140 μl (100 mg/ml stock in 0.15 M NaCl, 0.003 M KCl, 0.15 M KH_2PO_4, pH 7.4 [designated as PBS]) was added to produce a final PC-to-cholate molar ratio of ~1:1.6. Apo A-I (12.7 mg/ml) in 0.4 ml of PBS was added to the mixture, and the final volume was adjusted to 2 ml with PBS. The lipid-protein-cholate mixture was then incubated for 12 hours at 4°C, followed by dialysis against 2 L of PBS, for 2 days, with three buffer changes. Stability of the formulation was determined using RiboGreen assay (Quant-iT Ribogreen Kit, Cat no. R11490; Invitrogen, Carlsbad, CA) in subsequent gel exclusion chromatography. The rHDL/targeted siRNA solution was then diluted in 0.9% normal saline to a concentration of 0.2 mg/kg siRNA/0.2 ml of rHDL solution. In addition, zeta potential of the rHDL nanoparticle was measured using Zeta Plus (Brookhaven Instrument Co, Novato,

CA). Briefly, 1 ml of nanoparticles was added to a 1-ml cuvette for the assessment of zeta potential of nanoparticles.

Transmission Electron Microscopy

After dialysis against 0.125 M ammonium acetate, 2.6 mM ammonium carbonate, 0.26 mM EDTA, pH 7.4, the rHDL samples were negatively stained with 2% sodium phosphotungstate, pH 7.2, and placed on Formvar/carbon–coated 200-mesh nickel grid support films (Ted Pella, Inc, Redding, CA). The particles were visualized (magnification of 50,000) using a Zeiss 910 transmission electron microscope (Carl Zeiss MicroImaging, LLC, Thornwood, NY). The photographs obtained were enhanced, and the particle diameter was determined with Adobe Imageready CS2 software (Adobe Systems, Inc, San Jose, CA).

Cell Lines and Culture Conditions

The derivation and source of human epithelial ovarian cancer cell lines HeyA8, SKOV3ip1, and HeyA8-MDR have been reported previously

[7–9,38]. Human colorectal cancer cell line (HCT116) was a generous gift from Dr Lee Ellis (University of Texas MD Anderson Cancer Center, Houston, TX). All cell lines used in this study were authenticated by the characterized cell line core at the University of Texas MD Anderson Cancer Center. Briefly, the HeyA8 and SKOV3ip1 cells were maintained in RPMI 1640 supplemented with 15% fetal bovine serum (FBS) and 0.1% gentamicin sulfate (Gemini Bio-Products, Woodland, CA). HeyA8-MDR cells were maintained in RPMI 1640 supplemented with 15% FBS, 300 ng/ml paclitaxel (Abraxis BioScience, Los Angeles, CA), and 0.1% gentamicin sulfate. HCT116 cells were kept in culture using Dulbecco modified Eagle medium supplemented with 10% FBS and 0.1% gentamicin sulfate. All cells were kept in 5% CO_2/95% air at 37°C [39].

In Vitro *Gene Silencing*

STAT3 (target sequence 5′-GCCUCUCUGCA GAAUUCAA-3′), FAK (target sequence 5′CCACCUGGGCCAGUAUUAU-3′), and a nontargeted control sequence (target sequence 5′-UUCUCCGAAC-GUGUCACGU-3′) were purchased from Sigma-Aldrich Corporation (Woodland, TX), and RNAiFect transfection reagent was used (Qiagen, Valencia, CA) as per the manufacturer's recommendations. Briefly, SKOV3ip1 and HeyA8-MDR ovarian cancer cells were transfected with 1.33 µg of specific siRNA/well in six-well plates in triplicates, at 70% confluence. Transfection was performed using the 1:3.75 of siRNA and transfection reagent, respectively, in serum-free medium for 6 hours with the following treatment groups: control siRNA and STAT3 siRNA.

RNA Extraction and Complementary DNA Preparation

Cells were homogenized with Trizol (Invitrogen, Carlsbad, CA). RNA was extracted (chloroform), precipitated (isopropanol), and purified (75% ethanol). cDNA was generated with 2.0 µg of high-quality RNA using SuperScript-II reverse transcriptase kit (Invitrogen) [40].

Microarray Analysis

cDNA microarray was performed using the Illumina platform (Illumina Inc, San Diego, CA) on SKOV3 cells that were treated in 10-cm cell culture plates with either STAT3 (8.0 µg) or control siRNA (8.0 µg) in triplicate using RNAiFect transfection reagent (Qiagen) as per the manufacturer's recommendations. STAT3 gene silencing was confirmed at the protein level using Western blot before the microarray analysis. Gene expression data from microarray analysis were then loaded into the IPA Ingenuity pathway database, and differentially expressed genes related to apoptosis were selected for validation.

Polymerase Chain Reaction Assay

Reverse transcription–polymerase chain reaction (RT-PCR) was preformed using cDNA from normal human organs and cancer cell lines. cDNA from human liver was used as a positive control for SR-B1 expression. Quantitative real-time PCR was performed in Applied Biosystems 9500 series using conditions that have been previously described [41] using SYBR Green Master Mix (Applied Biosystems, Foster City, CA) in triplicate. β-Actin was used as an endogenous control. Mean fold change is reported.

Western Blot Analysis

Cell lysates were prepared with modified radioimmune precipitation lysis buffer [42]. Proteins were separated on 8% SDS-PAGE and transferred to nitrocellulose membrane (Bio-Rad Laboratories, Philadelphia,

PA), followed by incubation with STAT3 (1:2500) or FAK (1:5000) antibodies (BD Biosciences, San Diego, CA) overnight at 4°C. Primary antibody was detected using antimouse immunoglobulin G (GE Healthcare, Buckinghamshire, England, UK) and developed with a chemiluminescence detection kit (Perkin-Elmer, Covina, CA). β-Actin (1:2000; Sigma) or vinculin (1:3000; Cell Signaling Technology, Inc, Danvers, MA) confirmed equal loading.

Apoptosis Assay in Ovarian Cancer Cell

Twenty-four hours after treatment with control siRNA or STAT3 siRNA, ovarian cancer cells (SKOV3ip1 and HeyA8-MDR) cells were treated with docetaxel (1 or 500 nM, respectively) for 72 hours (triplicate), washed, and incubated with 5 µl of Annexin V/PE and 7AAD antibodies (BD Pharmingen, San Diego, CA) for 30 minutes. Flow cytometry was then performed to analyze the samples as previously described [43].

Immunohistochemistry

Fresh-frozen (OCT) sections were stained for CD31 (1:800 dilution; Pharmingen) [7,44], and Ki-67 staining was performed on 5-µm-thick formalin-fixed paraffin-embedded specimens [8]. To quantify microvessel density (MVD), cell proliferation index (Ki-67), and cleaved caspase-3, five random 0.159-mm^2 fields were studied at 100× magnification for each tumor, and microvessel density percent Ki-67 and percent cleaved caspase-3–positive cells were counted [9]. SR-B1 expression in human epithelial ovarian tumors (n = 50) was determined [38] using paraffin-embedded human ovarian cancer specimens from the University of Texas MD Anderson Cancer Center's tumor bank after institutional review board approval. High *versus* low expression was determined by a gynecologic pathologist using the following procedures: intensity was scored from 1 to 3, and distribution was scored from 1 to 4. The product of the two values was used to determine the extent of the expression, and a score greater than 4 was considered a high expression.

TUNEL Staining

Fresh-frozen sections of tumor tissues from therapy experiments (SKOV3ip1 model) were stained by terminal deoxynucleotidyl transferase–mediated deoxyuridine triphosphate nick-end labeling (TUNEL; green; Promega, Madison, WI) [38] and counterstained with Hoechst 1:10,000 [44]. An apoptotic body was represented by green fluorescence. To quantify apoptotic cells, TUNEL-positive cells were calculated in 10 random fields at 200× from five separate slides per group. Average values are presented.

Selective Delivery of siRNA

Female nude mice bearing SKOV3ip1 tumors were injected intravenously (intravenously [IV] through the tail vein) or intraperitoneally (IP) with 0.2 mg/kg of fluorescently tagged (Alexa555) control siRNA (Sigma-Aldrich) or untagged control siRNA (n = 3 per group). Forty-eight hours later, mice were killed, and tumors and organs (brain, heart, lung, liver, kidney, and spleen) were collected and frozen in OCT.

Fluorescence Staining

Fresh-frozen tumor tissues from orthotopic ovarian cancer models (SKOV3ip1) were fixed in acetone, washed with PBS, and counterstained with Hoechst (1:10,000). Fluorescence microscopy was used to analyze slides at 400×. Ten high-power fields were analyzed per slide, and a mean is reported.

Orthotopic Ovarian Cancer Models

Female nude mice (10-12 weeks old) were obtained from the US National Cancer Institute. All experiments were approved by the Institutional Animal Care and Use Committee of the MD Anderson Cancer Center.

FAK Targeting In Vivo

For FAK targeting experiments (SKOV3ip1 model), treatment was given in the following groups (*n* = 10 per group): 1) empty rHDL nanoparticles, 2) control siRNA/rHDL, 3) FAK siRNA/rHDL, 4) control siRNA + docetaxel, and 5) FAK siRNA/rHDL + docetaxel.

STAT3 Targeting In Vivo

For STAT3 silencing experiments, treatment was given according to the following groups (*n* = 10 per group): 1) control siRNA/rHDL, 2) control siRNA/rHDL + docetaxel, 3) STAT3 siRNA/rHDL, and 4) STAT3 siRNA/rHDL plus docetaxel. Tumor cells from appropriate ovarian cancer mouse models (HeyA8, 2.5×10^5; SKOV3ip1 and HeyA8-MDR, 1.0×10^6) were injected intraperitoneally into mice on day 0. Mice were randomized and treatment was started on day 7. About 3 (HeyA8) or 5 weeks (SKOV3ip1 and HEYA8-MDR) later, mice were subjected to necropsy, and tumors were harvested.

Colorectal Cancer Metastasis Model

For colorectal cancer metastasis model, HCT116 cells (1.0×10^6) were injected into the spleen (*n* = 10 per treatment group) of female nude mice. Two weeks later, treatment with oxaliplatin was started as previously described [39], according to the groups shown in Figure 2*C*. After 4 weeks, mice were killed, and tumors were harvested.

In Vivo Dose-Finding Experiment

An effective dose required to silence STAT3 or FAK genes *in vivo* was determined by injecting doses ranging from 0.1 to 0.2 mg/kg of STAT3 siRNA/rHDL or FAK siRNA/rHDL in SKOV3ip1 tumor-bearing mice. Mice were subjected to necropsy on day 2, 4, or 6. Tumors were harvested, and protein expression was determined using Western blot analysis as described above.

Statistical Analysis

Continuous variables were compared using the Student's *t* test (between two groups) or analysis of variance (for all groups) if normally distributed. In nonparametric values, continuous variables were compared with the use of the Mann-Whitney rank sum test or Kruskal-Wallis test (for all groups). For *in vivo* rHDL therapy studies, 10 mice per treatment group were randomly assigned. Thus, our sample size provided 80% power to detect a 50% reduction in tumor weight at 5% level of statistical significance. We performed all statistical tests using SPSS (SPSS, Inc, Chicago, IL) and GraphPad Prism 5 software (GraphPad software, Inc, La Jolla, CA). We considered $P < .05$ to be significant. All statistical tests performed in this study were two-tailed.

Results

Preparation of RNAi Containing rHDL Nanoparticles

Because RNAi molecules are highly ionic, especially because of the presence of the negatively charged phosphate groups, we devised a novel formulation to incorporate siRNA into rHDL. Oligolysine peptides containing approximately 40 lysine residues provided the neutralizing component that allowed efficient incorporation (>90%) of siRNA molecules into rHDL. After siRNA incorporation, the rHDL nanoparticles have a diameter of ~10 nm (Figure 1, *A* and *B*) and possess a neutral charge (ζ potential, –3.2 mV). The rHDL nanoparticles were shown to have a robust payload carrying capacity (up to 4 mg of siRNA/ml). In addition, the siRNA containing nanoparticles were found to be exceptionally stable because no loss of siRNA was noted from rHDL complexes on 2 weeks of storage and redialysis of the samples.

SR-B1 Expression in Cancer Cells

Before testing the efficacy of rHDL as a delivery method for siRNA, we first analyzed multiple cell lines and human tumors for presence of the SR-B1 receptor. Among 50 human ovarian epithelial cancers, 96% of tumors expressed SR-B1 receptor (Figure 1*C*). In addition, we determined SR-B1 expression in normal human organs and in multiple breast, colorectal, pancreatic, and ovarian cancer cell lines using RT-PCR (Figure W1), and several cell lines were also examined with quantitative real-time PCR (Figure 1*D*). All of the cancer cell lines tested demonstrated high levels of SR-B1 expression. Among the normal tissues, only liver had high SR-B1 expression, whereas others had minimal to no expression.

Selective Delivery of rHDL Nanoparticles In Vivo

Given the high expression of SR-B1 in tumors compared with normal tissues [17], we next examined the efficiency of *in vivo* siRNA delivery using rHDL nanoparticles. Fluorescently tagged (Alexa555) siRNA was incorporated into rHDL nanoparticles and injected IV or IP (Figure 2*A*). After a single injection, the siRNA was distributed evenly to ~80% of a given tumor. We further asked whether the rHDL particle delivery was receptor mediated. To address this question, we first analyzed organs from mice that were treated with the Alexa555-tagged siRNA/rHDL (Figure W2). Highest uptake of rHDL nanoparticles was noted in the liver, whereas minimal to no delivery was noted in brain, heart, lung, kidney, or spleen. In addition, there were no significant differences in tumor uptake of rHDL particles after intraperitoneal *versus* intravenous administration of rHDL/Alexa555 (Figure W2).

Before conducting long-term therapy experiments with this approach, we next examined the efficacy of STAT3 siRNA incorporated into rHDL nanoparticles (siRNA/rHDL) for gene silencing *in vivo*. STAT3 siRNA efficacy was first tested *in vitro* (Figure W3*A*) in SKOV3 cells where 5 μg of STAT3 siRNA resulted in greater than 80% reduction in STAT3 protein expression compared with control siRNA. Next, to determine an effective dose required to silence STAT3 *in vivo*, we injected doses ranging from 0.1 to 0.2 mg/kg of STAT3 siRNA/rHDL in SKOV3ip1 tumor bearing mice. On day 4, after a single injection of 0.2 mg/kg of siRNA, we found 88% reduction in STAT3 protein levels (Figure W3*B*), with some return of expression by day 6. On the basis of this experiment, we used the 0.2-mg/kg dose for all subsequent studies. Similar results were noted (Figure W3*C*) with targeting another critical gene for cancer growth and metastasis, FAK [7]. FAK siRNA/rHDL resulted in 87% reduction in FAK levels on day 4 after a single injection of FAK siRNA incorporated into rHDL nanoparticles in nude mice bearing SKOV3ip1 tumors.

Effect of STAT3 or FAK Gene Silencing on Tumor Growth and Metastasis

After successfully silencing STAT3 or FAK genes *in vivo* (Figure W3*B* and *C*), we next tested the therapeutic efficacy of this approach with
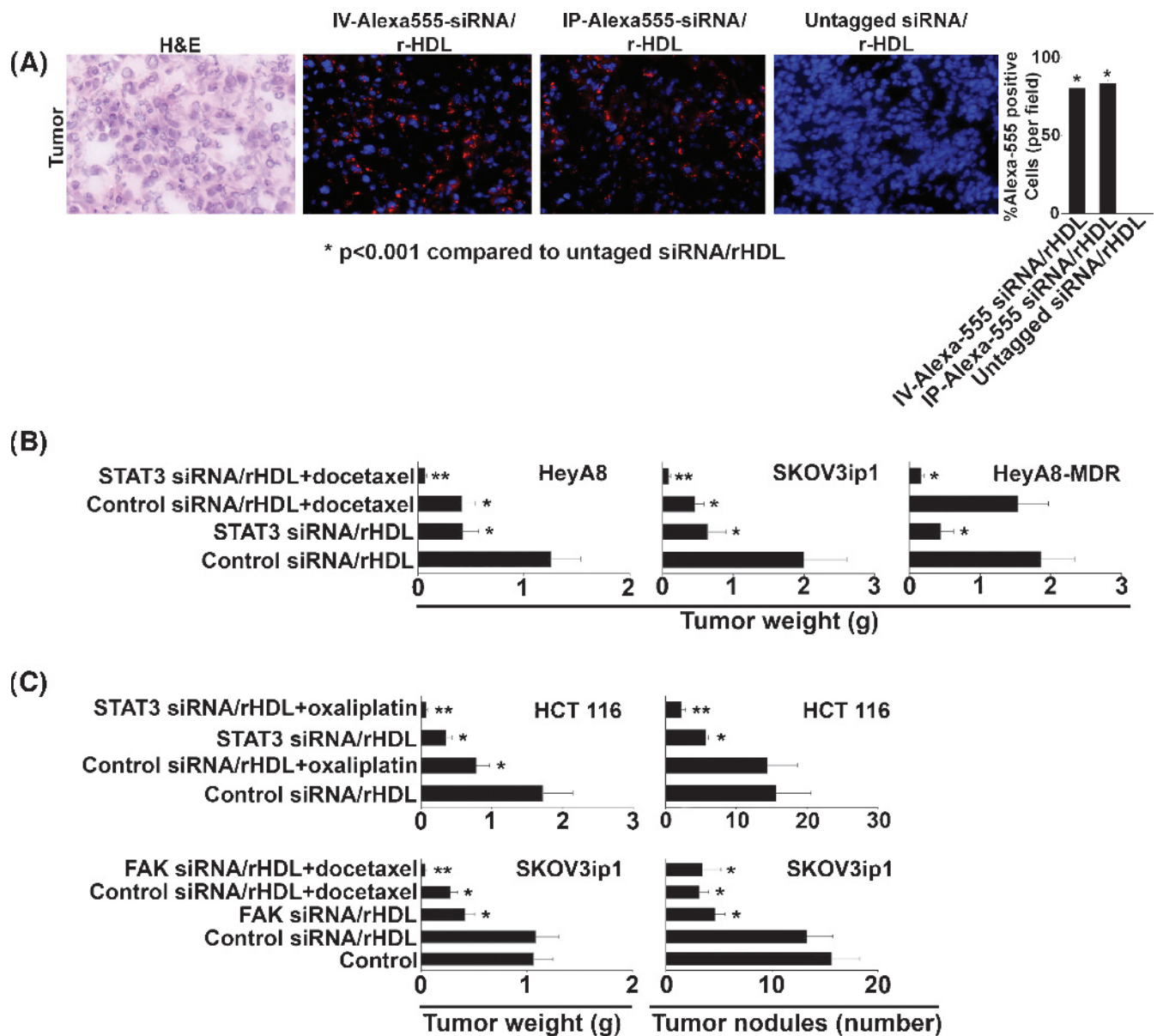
Figure 2. Systemic delivery of siRNA using rHDL nanoparticles. (A) Uptake of Alexa555-labeled siRNA/rHDL in SKOV3ip1 tumors. A single IV or IP injection of 0.2 mg/kg of Alexa555 labeled or 0.2 mg/kg of IV and IP injection of untagged siRNA/rHDL was administered in mice bearing SKOV3ip1 tumors, and 48 hours later, tumors were harvested and counterstained with Hoechst (blue), and siRNA (red) uptake was assessed with fluorescence microscopy. The H&E image shows tumor histologic diagnosis. The adjacent graph shows percent Alexa555-positive cells. (B) *In vivo* efficacy of STAT3 siRNA/rHDL in chemosensitive (HeyA8 and SKOV3ip1) and chemoresistant (HeyA8-MDR) mouse models of ovarian carcinoma. *$P < .05$ compared with controls. **$P < .05$ compared with controls as well as docetaxel alone. (C) *In vivo* efficacy of STAT3 siRNA/rHDL in colorectal cancer model of liver metastases (HCT116). *$P < .05$ compared with control siRNA/rHDL, **$P < .05$ compared with STAT3 or oxaliplatin alone. *In vivo* efficacy of FAK siRNA/rHDL in the SKOV3ip1 ovarian cancer model. *$P < .05$ compared with controls. **$P < .05$ compared with controls as well as docetaxel alone. Error bars, SEM.

or without docetaxel chemotherapy. We first targeted STAT3 using STAT3 siRNA/rHDL (Figure 2B). Mice were treated with either STAT3 siRNA/rHDL alone or in combination with docetaxel using three well-characterized orthotopic mouse models of ovarian cancer. In the HeyA8 model, STAT3 siRNA/rHDL or docetaxel monotherapy reduced tumor weight by 62% ($P < .05$, both). Combination treatment with STAT3 siRNA/rHDL and docetaxel resulted in the greatest reduction in tumor weight (by 92%, $P < .05$) compared with controls. Similar results were noted in the SKOV3ip1 model (Figure 2B). In addition, both HeyA8 and SKOV3ip1 ovarian cancer models demonstrated sizeable reductions

in the number of tumor nodules when mice were treated with STAT3 siRNA/rHDL with and without docetaxel therapy (Figure W4A).

Given that STAT3 is known to play a role in chemoresistance [45–48], we also performed experiments in the taxane-resistant HeyA8-MDR model (Figure 2B). As expected, docetaxel had no significant effect on tumor growth. STAT3 siRNA/rHDL monotherapy resulted in 76% reduction in tumor growth ($P < .01$). Combination of docetaxel with STAT3 siRNA/rHDL resulted in even greater reduction in tumor growth (by 91%, $P < .001$, compared with control and by 89%, $P < .001$, compared with docetaxel). Similar effects were seen on number

of tumor nodules (Figure W4*B*). We also analyzed the frequency of metastasis by location in animals in each treatment group (Figure W4*B*). Compared with control and docetaxel monotherapy groups, STAT3 siRNA/rHDL alone or in combination with docetaxel resulted in a substantial reduction in upper abdominal and parenchymal liver metastasis.

Next, we examined the therapeutic effect of STAT3 gene silencing in a well-characterized mouse model of metastatic colorectal cancer (HCT116) [39] that has high baseline SR-B1 expression (Figure 2*C*). After tumor cell injection into the spleen, there is metastatic spread to the liver in this model. STAT3 siRNA/rHDL treatment alone resulted in 79% reduction in tumor weight ($P < .01$). For these experiments, we used the commonly used cytotoxic, oxaliplatin, in combination with STAT3 siRNA/rHDL. Oxaliplatin reduced tumor growth by 55% ($P < .01$). The combination of oxaliplatin and STAT3 siRNA/rHDL resulted in the most significant reduction in tumor weight (96%, $P < .01$) and the number of metastatic lesions in the liver (86%, $P < .01$) compared with controls. To assess the safety of rHDL nanoparticles, we assessed several parameters in mice treated with rHDL nanoparticles (Figure W5). There were no significant differences in animal body weight or liver function tests (AST and ALT ratio) between different treatment groups (Figure W5, *A* and *B*). Hematoxylin and eosin (H&E) staining of multiple normal organs after therapy experiments revealed no significant changes compared with the control group (Figure W5*C*).

To test the potential utility of rHDL nanoparticles against other targets, we carried out additional experiments with FAK siRNA/rHDL. Here, we targeted FAK using FAK siRNA/rHDL in the SKOV3ip1 orthotopic model of ovarian carcinoma (Figure 2*C*). FAK or docetaxel monotherapy resulted in 62% and 74% reduction in tumor weight ($P < .01$, both). The combination treatment resulted in the greatest

reduction in tumor weight (by 96%, $P < .01$) and the number of tumor nodules (by 74%, $P < .05$). There were no significant differences in tumor weights or number of tumor nodules between mice that were treated with empty rHDL nanoparticles *versus* those treated with control siRNA/rHDL.

Effect of STAT3 Targeting on Tumor Microenvironment

To understand the biologic effects of STAT3/rHDL treatment, a series of *in vitro* and *in vivo* experiments were carried out using both chemosensitive (SKOV3ip1) and chemoresistant (HeyA8-MDR) ovarian cancer models. In the SKOV3ip1 ovarian cancer model (Figure 3), STAT3 gene silencing alone resulted in a 26% reduction in cell proliferation ($P < .05$), whereas docetaxel inhibited tumor cell proliferation by 30% ($P < .05$). Combination treatment with STAT3 siRNA/rHDL and docetaxel reduced tumor cell proliferation by 48% ($P < .05$) compared with controls (Figure 3). In the HeyA8-MDR ovarian cancer model (Figure W6), where docetaxel treatment alone had no effect on cell proliferation, STAT3 siRNA/rHDL monotherapy resulted in 19% reduction in proliferation. Combination of STAT3 siRNA/rHDL and docetaxel resulted in most significant reduction (39%, $P < .05$) compared with the control treatment (Figure W6).

To ascertain the effects of STAT3 silencing on tumor-associated angiogenesis, we performed CD31 staining on fresh-frozen tumor samples from all four treatment groups (Figures 3 and W6) and determined MVD. In the SKOV3ip1 model, STAT3 siRNA/rHDL or docetaxel monotherapy resulted in 66% to 69% reduction ($P < .05$, both) in MVD (Figure 3). The combination of STAT3 siRNA/rHDL and docetaxel resulted in 88% reduction in MVD ($P < .05$) compared
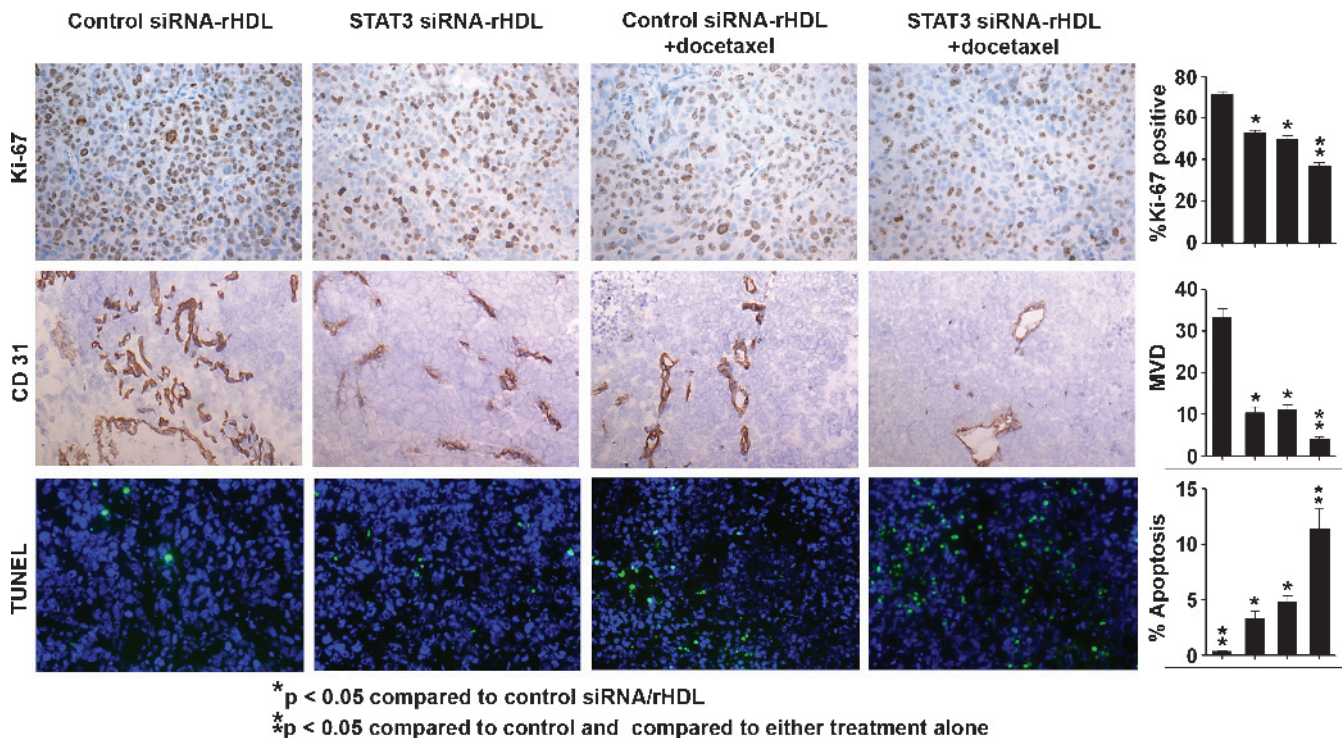

Figure 3. Effect of rHDL-incorporated STAT3 siRNA on tumor microenvironment. Tissues harvested after STAT3 siRNA/rHDL therapy were subjected to immunohistochemistry for markers of proliferation (Ki-67), angiogenesis (CD 31), and apoptosis (TUNEL). For the TUNEL stain, five random fields per slide were examined with fluorescence microscopy, and the number of apoptotic bodies and nuclei is reported as average percent apoptotic cells (200×). Error bars, SEM.
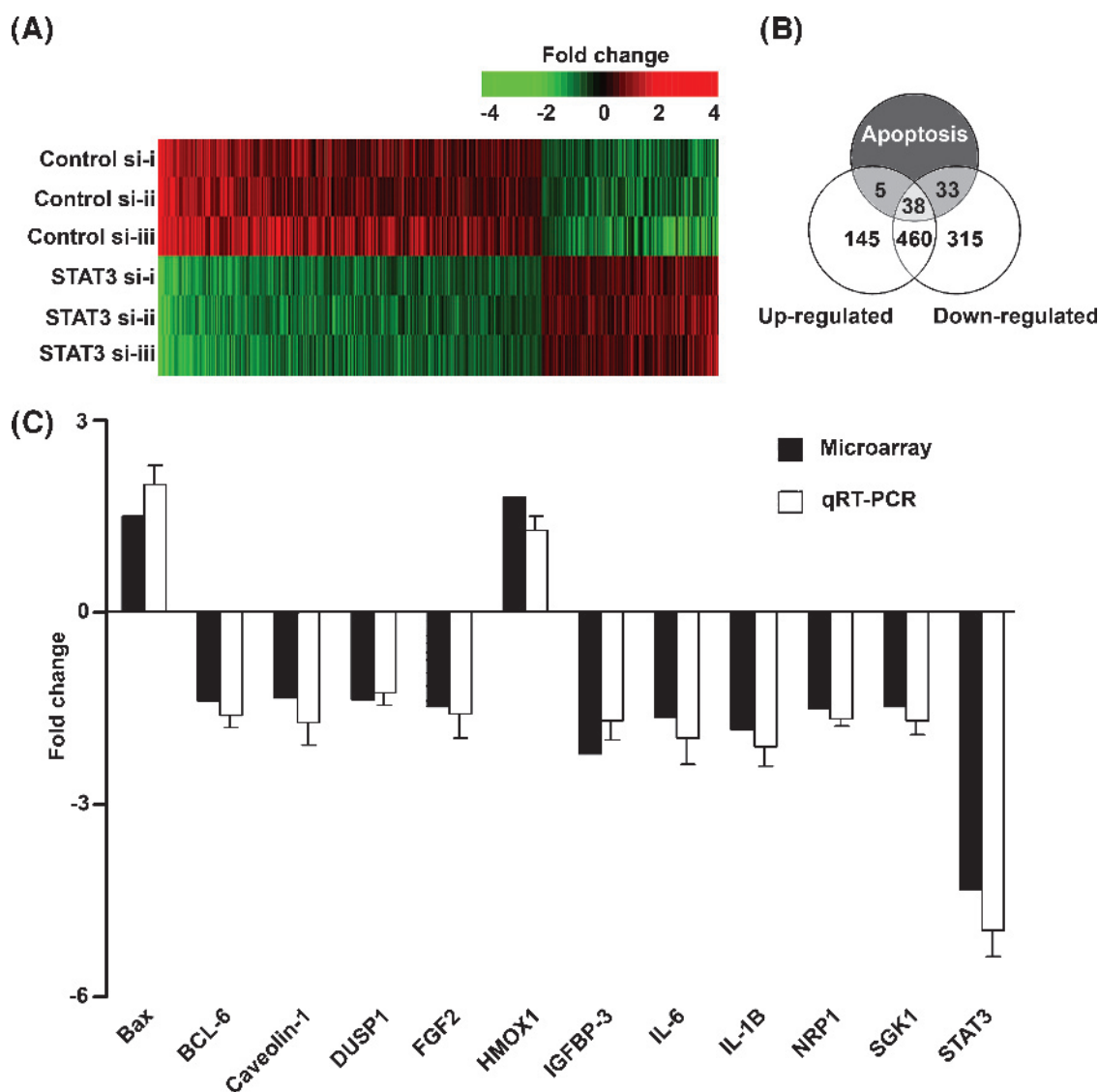
Figure 4. Effect of STAT3 silencing on gene expression profile of ovarian cancer cells. (A) STAT3 silencing modulates gene expression of apoptosis related genes. After STAT3 silencing with siRNA (*in vitro*), microarray analysis was performed. Heat map (A) represents the over all gene expression changes. Analysis of apoptosis-related (B) genes are shown. (C) Validation of microarray. Apoptosis-related genes that were differentially expressed between control siRNA and STAT3 siRNA treatment groups were validated with quantitative real-time RT-PCR. Average fold change is presented. Error bars, SEM.

with controls. Similarly, in the HeyA8-MDR model, docetaxel treatment alone had no effect on MVD, but the combination of docetaxel with STAT3 siRNA/rHDL resulted in a substantial reduction (Figure W6).

STAT3 is known to increase cell survival and inhibit apoptosis [45–48]. Therefore, we also examined effects on tumor cell apoptosis using TUNEL staining in the SKOV3ip1 ovarian cancer treatment model (Figure 3) and cleaved caspase-3 staining in the HeyA8-MDR model (Figure W6). In the SKOV3ip1 model, STAT3 gene silencing or docetaxel treatment resulted in 8- to 12-fold increase in apoptosis compared with controls ($P < .05$, both). Combination treatment with STAT3 siRNA/rHDL and docetaxel resulted in a 30-fold increase in tumor cell apoptosis compared with the control group ($P < .05$). In addition, in the HeyA8-MDR model, docetaxel treatment alone had no effect on apoptosis, but treatment with STAT3 siRNA/rHDL alone or combination treatment with STAT3 siRNA/rHDL and docetaxel resulted in substantial increase (by 61% and 76%, respectively, $P < .05$ for

both) in apoptotic cells (cleaved caspase-3–positive) compared with control siRNA/rHDL treatment (Figure W6).

Tissue-Based Markers of STAT3 Silencing in Ovarian Cancer Cells

To identify potential tissue-based markers of response to STAT3 gene silencing, we performed genomic analyses on control *versus* STAT3 siRNA-treated ovarian cancer cells (Figure 4, *A* and *B*). There were 460 genes that were differentially expressed between these two groups. Given that the biologic data pointed toward apoptosis and impaired cell survival as the dominant effects after STAT3 silencing, we focused on genes in these pathways (Table W1). From this list, we validated 12 genes that were most significantly altered with STAT3 gene silencing (Figure 4*C*) using quantitative real-time RT-PCR. The extent of STAT3 gene silencing was consistent between the two modalities. STAT3 silencing resulted in substantial decreases in key survival genes

that are known to regulate MAP kinase and AKT pathway (Figure 4C). These genes may serve as important tissue-based markers of response to STAT3-targeted therapy. Similar changes were noted in the HeyA8-MDR model (data not shown).

Effects of In Vitro STAT3 Silencing on Apoptosis

To determine whether the effects of STAT3 gene silencing on tumor cell apoptosis were direct, we examined the effects of STAT3 siRNA with or without docetaxel on ovarian cancer cell (SKOV3ip1 and HeyA8-MDR) viability (Figure 5). STAT3 silencing was confirmed with Western blot analysis (Figure W3A). In SKOV3ip1 cells, STAT3 siRNA or docetaxel monotherapy resulted in increased apoptosis (by

Figure 5. Effect of STAT3 silencing on apoptosis. STAT3 was silenced using STAT3-specific siRNA in (A) SKOV3ip1 and (B) HeyA8-MDR cells with and without docetaxel treatment, and apoptosis was assessed using flow cytometry (annexin V). Average percent apoptosis (Annexin V/PE–positive SKOV3 cells) and average percent apoptosis compared with control (annexin V/PE–positive HeyA8-MDR cells) are reported. Error bars, SEM.

3- and 5.2-fold, respectively, $P < .05$, both), whereas the combination treatment resulted in 7.7-fold higher apoptosis compared with control ($P < .05$). Compared with docetaxel treatment, the addition of STAT3 siRNA resulted in 41% greater apoptosis ($P < .05$), suggesting that the observed *in vivo* apoptotic effects were indeed direct (Figure 5A). In addition, docetaxel treatment in HeyA8-MDR cells (Figure 5B) did not result in any significant apoptosis. However, exposure to docetaxel after STAT3 silencing resulted in 175% increase ($P < .05$) in apoptosis compared with controls and 98% higher apoptosis ($P < .05$) compared with docetaxel treatment alone.

Discussion

The key findings of this study are that rHDL nanoparticles can efficiently deliver siRNA *in vivo* to silence genes that are critical for cancer growth and progression. This concept was illustrated by the highly effective STAT3 or FAK gene silencing in multiple tumor models through siRNA incorporated into rHDL nanoparticles. The biologic effects were mediated by decreased tumor cell proliferation, reduction in angiogenesis, and decreased cell survival.

Although RNA interference is a highly specific mode of gene silencing, its therapeutic application is currently limited due primarily to difficulties in systemic *in vivo* delivery [49–51]. To overcome these barriers, selective biocompatible delivery systems are needed. To date, several nanoparticle systems have been used for potential therapeutic interventions [11,12,52]; however, majority of these systems may result in toxicities to normal tissues due to lack of tissue specificity and wide body distribution [52,53]. Consequently, nonspecific delivery systems may require higher doses to accomplish effective and sustained gene silencing. Therefore, targeted delivery is highly desirable to overcome the hurdles seen with other approaches [54].

There are many advantages of using rHDL as a delivery system for siRNA. For example, cellular uptake of the rHDL core components is considered to occur through a specific receptor (SR-B1), which allows selective siRNA delivery. Our data show that SR-B1 receptor expression is increased in tumor cells compared with most normal tissues. This differential expression may help in avoiding undesired side effects. In the current study, uptake of rHDL nanoparticles was largely restricted to the tumor and liver. This pattern of uptake is entirely consistent with the distribution of SR-B1 expression [24]. In addition, our safety studies indicate that STAT3/rHDL uptake in the liver did not result in any adverse effects in mice compared with the control siRNA treatment group.

For proof-of-concept, we demonstrated successful therapeutic targeting of two important genes for cancer growth and progression in multiple preclinical models. STAT3 is a well-characterized transcription factor that is involved in many key processes implicated in cancer progression and metastasis [55,56]. RNA interference is attractive as a therapeutic strategy, especially against targets that are not easily "druggable" by other methods. Although STAT3 is widely considered to be an important cancer promoter, conventional approaches are limited for its targeting [57]. Therefore, siRNA delivery, as shown here, is an important approach for targeting STAT3 and other important facilitators of malignant growth. The biologic effects of reduced angiogenesis, secondary to STAT3 silencing in tumor cells, is supported by several reports demonstrating that vascular endothelial growth factor expression is modulated by STAT3 activation [58]. Constitutively activated STAT3 in tumor cells correlates with increased vascular endothelial growth factor expression [59,60]. Consequently, targeting STAT3 for
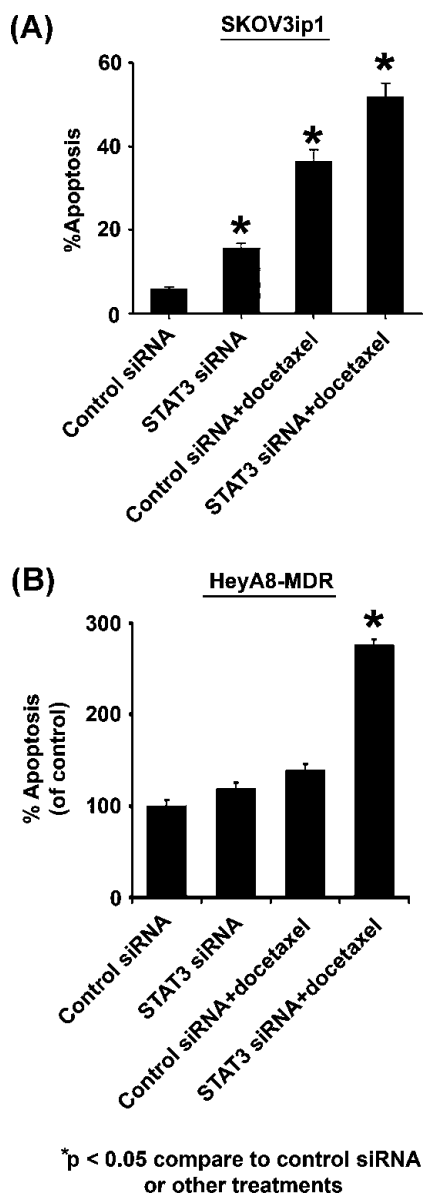
pharmacological intervention is now possible using the nanotechnology approaches described here.

In addition, among other solid tumors, FAK has also been reported to be over expressed in colorectal, breast, ovarian, thyroid, and prostate carcinoma [35,61–64], and in patients with ovarian cancer, overexpression of FAK is associated with aggressive tumor features resulting in poor over all survival [35]. Systemic targeting of FAK with liposomal nanoparticles or small molecule inhibitors has shown reduction in tumor growth and metastasis [7,38], but such approaches are not tumor-specific and could result in toxicities. FAK siRNA/rHDL treatment is highly tumor specific and resulted in significant reduction in tumor growth and metastasis without any obvious effects on other organs.

In summary, systemic siRNA delivery using rHDL nanoparticles opens new horizons for treatment of human malignancies. This delivery method not only is highly efficient but also allows for selectivity and biocompatibility. Thus, rHDL nanoparticles may have significant implications for cancer management.

Acknowledgments

References

[1] Elbashir SM, Harborth J, Lendeckel W, Yalcin A, Weber K, and Tuschl T (2001). Duplexes of 21-nucleotide RNAs mediate RNA interference in cultured mammalian cells. *Nature* **411**, 494–498.

[2] Fire A, Xu S, Montgomery MK, Kostas SA, Driver SE, and Mello CC (1998). Potent and specific genetic interference by double-stranded RNA in *Caenorhabditis elegans*. *Nature* **391**, 806–811.

[3] Hannon GJ and Rossi JJ (2004). Unlocking the potential of the human genome with RNA interference. *Nature* **431**, 371–378.

[4] Aagaard L and Rossi JJ (2007). RNAi therapeutics: principles, prospects and challenges. *Adv Drug Deliv Rev* **59**, 75–86.

[5] Merritt WM, Lin YG, Han LY, Kamat AA, Spannuth WA, Schmandt R, Urbauer D, Pennacchio LA, Cheng JF, Nick AM, et al. (2008). Dicer, Drosha, and outcomes in patients with ovarian cancer. *N Engl J Med* **359**, 2641–2650.

[6] Whitehead KA, Langer R, and Anderson DG (2009). Knocking down barriers: advances in siRNA delivery. *Nat Rev Drug Discov* **8**, 129–138.

[7] Halder J, Kamat AA, Landen CN Jr, Han LY, Lutgendorf SK, Lin YG, Merritt WM, Jennings NB, Chavez-Reyes A, Coleman RL, et al. (2006). Focal adhesion kinase targeting using *in vivo* short interfering RNA delivery in neutral liposomes for ovarian carcinoma therapy. *Clin Cancer Res* **12**, 4916–4924.

[8] Merritt WM, Lin YG, Spannuth WA, Fletcher MS, Kamat AA, Han LY, Landen CN, Jennings N, De Geest K, Langley RR, et al. (2008). Effect of interleukin-8 gene silencing with liposome-encapsulated small interfering RNA on ovarian cancer cell growth. *J Natl Cancer Inst* **100**, 359–372.

[9] Thaker PH, Han LY, Kamat AA, Arevalo JM, Takahashi R, Lu C, Jennings NB, Armaiz-Pena G, Bankson JA, Ravoori M, et al. (2006). Chronic stress promotes tumor growth and angiogenesis in a mouse model of ovarian carcinoma. *Nat Med* **12**, 939–944.

[10] Pirollo KF and Chang EH (2008). Targeted delivery of small interfering RNA: approaching effective cancer therapies. *Cancer Res* **68**, 1247–1250.

[11] Wolfrum C, Shi S, Jayaprakash KN, Jayaraman M, Wang G, Pandey RK, Rajeev KG, Nakayama T, Charrise K, Ndungo EM, et al. (2007). Mechanisms and optimization of *in vivo* delivery of lipophilic siRNAs. *Nat Biotechnol* **25**, 1149–1157.

[12] Zhang C, Jugold M, Woenne EC, Lammers T, Morgenstern B, Mueller MM, Zentgraf H, Bock M, Eisenhut M, Semmler W, et al. (2007). Specific targeting of tumor angiogenesis by RGD-conjugated ultrasmall superparamagnetic iron oxide particles using a clinical 1.5-T magnetic resonance scanner. *Cancer Res* **67**, 1555–1562.

[13] Schmitz G and Grandl M (2009). The molecular mechanisms of HDL and associated vesicular trafficking mechanisms to mediate cellular lipid homeostasis. *Arterioscler Thromb Vasc Biol* **29**, 1718–1722.

[14] Pussinen PJ, Lindner H, Glatter O, Reicher H, Kostner GM, Wintersperger A, Malle E, and Sattler W (2000). Lipoprotein-associated α-tocopheryl-succinate inhibits cell growth and induces apoptosis in human MCF-7 and HBL-100 breast cancer cells. *Biochim Biophys Acta* **1485**, 129–144.

[15] Connelly MA and Williams DL (2004). SR-BI and HDL cholesteryl ester metabolism. *Endocr Res* **30**, 697–703.

[16] Connelly MA and Williams DL (2004). Scavenger receptor BI: a scavenger receptor with a mission to transport high density lipoprotein lipids. *Curr Opin Lipidol* **15**, 287–295.

[17] Leon CG, Locke JA, Adomat HH, Etinger SL, Twiddy AL, Neumann RD, Nelson CC, Guns ES, and Wasan KM (2010). Alterations in cholesterol regulation contribute to the production of intratumoral androgens during progression to castration-resistant prostate cancer in a mouse xenograft model. *Prostate* **70**(4), 390–400.

[18] Lacko AG, Stewart DR, McClain R, Prokai L, and McConathy WJ (2007). Recent developments and patenting of lipoprotein based formulations. *Recent Pat Drug Deliv Formul* **1**, 143–145.

[19] Lacko AG, Nair M, Prokai L, and McConathy WJ (2007). Prospects and challenges of the development of lipoprotein-based formulations for anti-cancer drugs. *Expert Opin Drug Deliv* **4**, 665–675.

[20] Lacko AG, Nair M, Paranjape S, Johnso S, and McConathy WJ (2002). High density lipoprotein complexes as delivery vehicles for anticancer drugs. *Anticancer Res* **22**, 2045–2049.

[21] Kamaly N, Kalber T, Thanou M, Bell JD, and Miller AD (2009). Folate receptor targeted bimodal liposomes for tumor magnetic resonance imaging. *Bioconjug Chem* **20**, 648–655.

[22] Rigotti A, Miettinen HE, and Krieger M (2003). The role of the high-density lipoprotein receptor SR-BI in the lipid metabolism of endocrine and other tissues. *Endocr Rev* **24**, 357–387.

[23] Fenske SA, Yesilaltay A, Pal R, Daniels K, Barker C, Quinones V, Rigotti A, Krieger M, and Kocher O (2009). Normal hepatic cell surface localization of the high density lipoprotein receptor, scavenger receptor class B, type I, depends on all four PDZ domains of PDZK1. *J Biol Chem* **284**, 5797–5806.

[24] Mooberry LK, Nair M, Paranjape S, McConathy WJ, and Lacko AG (2010). Receptor mediated uptake of paclitaxel from a synthetic high density lipoprotein nanocarrier. *J Drug Target* **18**, 53–58.

[25] Feng M, Cai Q, Shi X, Huang H, Zhou P, and Guo X (2008). Recombinant high-density lipoprotein complex as a targeting system of nosiheptide to liver cells. *J Drug Target* **16**, 502–508.

[26] Acton S, Rigotti A, Landschulz KT, Xu S, Hobbs HH, and Krieger M (1996). Identification of scavenger receptor SR-BI as a high density lipoprotein receptor. *Science* **271**, 518–520.

[27] Pecot CV, Calin GA, Coleman RL, Lopez-Berestein G, and Sood AK (2010). RNA interference in the clinic: challenges and future directions. *Nat Rev Cancer* **11**, 59–67.

[28] Darnell JE Jr (1997). STATs and gene regulation. *Science* **277**, 1630–1635.

[29] Turkson J (2004). STAT proteins as novel targets for cancer drug discovery. *Expert Opin Ther Targets* **8**, 409–422.

[30] Yue P and Turkson J (2009). Targeting STAT3 in cancer: how successful are we? *Expert Opin Investig Drugs* **18**, 45–56.

[31] Hsia DA, Mitra SK, Hauck CR, Streblow DN, Nelson JA, Ilic D, Huang S, Li E, Nemerow GR, Leng J, et al. (2003). Differential regulation of cell motility and invasion by FAK. *J Cell Biol* **160**, 753–767.

[32] Kohno M, Hasegawa H, Miyake M, Yamamoto T, and Fujita S (2002). CD151 enhances cell motility and metastasis of cancer cells in the presence of focal adhesion kinase. *Int J Cancer* **97**, 336–343.

[33] Schaller MD (1996). The focal adhesion kinase. *J Endocrinol* **150**, 1–7.

[34] Sieg DJ, Hauck CR, Ilic D, Klingbeil CK, Schaefer E, Damsky CH, and Schlaepfer DD (2000). FAK integrates growth-factor and integrin signals to promote cell migration. *Nat Cell Biol* **2**, 249–256.

[35] Sood AK, Coffin JE, Schneider GB, Fletcher MS, DeYoung BR, Gruman LM, Gershenson DM, Schaller MD, and Hendrix MJ (2004). Biological significance of focal adhesion kinase in ovarian cancer: role in migration and invasion. *Am J Pathol* **165**, 1087–1095.

[36] McConathy WJ, Nair MP, Paranjape S, Mooberry L, and Lacko AG (2008). Evaluation of synthetic/reconstituted high-density lipoproteins as delivery vehicles for paclitaxel. *Anticancer Drugs* **19**, 183–188.

[37] Ryan RO, Forte TM, and Oda MN (2003). Optimized bacterial expression of human apolipoprotein A-I. *Protein Expr Purif* **27**, 98–103.

[38] Shahzad MM, Lu C, Lee JW, Stone RL, Mitra R, Mangala LS, Lu Y, Baggerly KA, Danes CG, Nick AM, et al. (2009). Dual targeting of EphA2 and FAK in ovarian carcinoma. *Cancer Biol Ther* **8**, 1027–1034.

[39] Kopetz S, Lesslie DP, Dallas NA, Park SI, Johnson M, Parikh NU, Kim MP, Abbruzzese JL, Ellis LM, Chandra J, et al. (2009). Synergistic activity of the SRC family kinase inhibitor dasatinib and oxaliplatin in colon carcinoma cells is mediated by oxidative stress. *Cancer Res* **69**, 3842–3849.

[40] Halder J, Landen CN Jr, Lutgendorf SK, Li Y, Jennings NB, Fan D, Nelkin GM, Schmandt R, Schaller MD, and Sood AK (2005). Focal adhesion kinase silencing augments docetaxel-mediated apoptosis in ovarian cancer cells. *Clin Cancer Res* **11**, 8829–8836.

[41] Lu C, Han HD, Mangala LS, Ali-Fehmi R, Newton CS, Ozbun L, Armaiz-Pena GN, Hu W, Stone RL, Munkarah A, et al. (2010). Regulation of tumor angiogenesis by EZH2. *Cancer Cell* **18**, 185–197.

[42] Landen CN Jr, Lu C, Han LY, Coffman KT, Bruckheimer E, Halder J, Mangala LS, Merritt WM, Lin YG, Gao C, et al. (2006). Efficacy and antivascular effects of EphA2 reduction with an agonistic antibody in ovarian cancer. *J Natl Cancer Inst* **98**, 1558–1570.

[43] Lee JW, Han HD, Shahzad MM, Kim SW, Mangala LS, Nick AM, Lu C, Langley RR, Schmandt R, Kim HS, et al. (2009). EphA2 immunoconjugate as molecularly targeted chemotherapy for ovarian carcinoma. *J Natl Cancer Inst* **101**, 1193–1205.

[44] Thaker PH, Yazici S, Nilsson MB, Yokoi K, Tsan RZ, He J, Kim SJ, Fidler IJ, and Sood AK (2005). Antivascular therapy for orthotopic human ovarian carcinoma through blockade of the vascular endothelial growth factor and epidermal growth factor receptors. *Clin Cancer Res* **11**, 4923–4933.

[45] Shen Y, Devgan G, Darnell JE Jr, and Bromberg JF (2001). Constitutively activated Stat3 protects fibroblasts from serum withdrawal and UV-induced apoptosis and antagonizes the proapoptotic effects of activated Stat1. *Proc Natl Acad Sci USA* **98**, 1543–1548.

[46] Catlett-Falcone R, Landowski TH, Oshiro MM, Turkson J, Levitzki A, Savino R, Ciliberto G, Moscinski L, Fernandez-Luna JL, Nunez G, et al. (1999). Constitutive activation of Stat3 signaling confers resistance to apoptosis in human U266 myeloma cells. *Immunity* **10**, 105–115.

[47] Zushi S, Shinomura Y, Kiyohara T, Miyazaki Y, Kondo S, Sugimachi M, Higashimoto Y, Kanayama S, and Matsuzawa Y (1998). STAT3 mediates the survival signal in oncogenic *ras*-transfected intestinal epithelial cells. *Int J Cancer* **78**, 326–330.

[48] Masuda M, Suzui M, Yasumatu R, Nakashima T, Kuratomi Y, Azuma K, Tomita K, Komiyama S, and Weinstein IB (2002). Constitutive activation of signal transducers and activators of transcription 3 correlates with cyclin D1 overexpression and may provide a novel prognostic marker in head and neck squamous cell carcinoma. *Cancer Res* **62**, 3351–3355.

[49] Lu PY, Xie F, and Woodle MC (2005). *In vivo* application of RNA interference: from functional genomics to therapeutics. *Adv Genet* **54**, 117–142.

[50] Sioud M (2005). On the delivery of small interfering RNAs into mammalian cells. *Expert Opin Drug Deliv* **2**, 639–651.

[51] Schiffelers RM, Woodle MC, and Scaria P (2004). Pharmaceutical prospects for RNA interference. *Pharm Res* **21**, 1–7.

[52] Landen CN Jr, Chavez-Reyes A, Bucana C, Schmandt R, Deavers MT, Lopez-Berestein G, and Sood AK (2005). Therapeutic EphA2 gene targeting *in vivo* using neutral liposomal small interfering RNA delivery. *Cancer Res* **65**, 6910–6918.

[53] Soutschek J, Akinc A, Bramlage B, Charisse K, Constien R, Donoghue M, Elbashir S, Geick A, Hadwiger P, Harborth J, et al. (2004). Therapeutic silencing of an endogenous gene by systemic administration of modified siRNAs. *Nature* **432**, 173–178.

[54] Das M, Mohanty C, and Sahoo SK (2009). Ligand-based targeted therapy for cancer tissue. *Expert Opin Drug Deliv* **6**, 285–304.

[55] Gamero AM, Young HA, and Wiltrout RH (2004). Inactivation of Stat3 in tumor cells: releasing a brake on immune responses against cancer? *Cancer Cell* **5**, 111–112.

[56] Kortylewski M, Kujawski M, Wang T, Wei S, Zhang S, Pilon-Thomas S, Niu G, Kay H, Mule J, Kerr WG, et al. (2005). Inhibiting Stat3 signaling in the hematopoietic system elicits multicomponent antitumor immunity. *Nat Med* **11**, 1314–1321.

[57] Lin L, Amin R, Gallicano GI, Glasgow E, Jogunoori W, Jessup JM, Zasloff M, Marshall JL, Shetty K, Johnson L, et al. (2009). The STAT3 inhibitor NSC 74859 is effective in hepatocellular cancers with disrupted TGF-β signaling. *Oncogene* **28**, 961–972.

[58] Niu G, Wright KL, Huang M, Song L, Haura E, Turkson J, Zhang S, Wang T, Sinibaldi D, Coppola D, et al. (2002). Constitutive Stat3 activity up-regulates VEGF expression and tumor angiogenesis. *Oncogene* **21**, 2000–2008.

[59] Wei D, Le X, Zheng L, Wang L, Frey JA, Gao AC, Peng Z, Huang S, Xiong HQ, Abbruzzese JL, et al. (2003). Stat3 activation regulates the expression of vascular endothelial growth factor and human pancreatic cancer angiogenesis and metastasis. *Oncogene* **22**, 319–329.

[60] Wei LH, Kuo ML, Chen CA, Chou CH, Lai KB, Lee CN, and Hsieh CY (2003). Interleukin-6 promotes cervical tumor growth by VEGF-dependent angiogenesis via a STAT3 pathway. *Oncogene* **22**, 1517–1527.

[61] Ayaki M, Komatsu K, Mukai M, Murata K, Kameyama M, Ishiguro S, Miyoshi J, Tatsuta M, and Nakamura H (2001). Reduced expression of focal adhesion kinase in liver metastases compared with matched primary human colorectal adenocarcinomas. *Clin Cancer Res* **7**, 3106–3112.

[62] Cance WG, Harris JE, Iacocca MV, Roche E, Yang X, Chang J, Simkins S, and Xu L (2000). Immunohistochemical analyses of focal adhesion kinase expression in benign and malignant human breast and colon tissues: correlation with preinvasive and invasive phenotypes. *Clin Cancer Res* **6**, 2417–2423.

[63] Owens LV, Xu L, Craven RJ, Dent GA, Weiner TM, Kornberg L, Liu ET, and Cance WG (1995). Overexpression of the focal adhesion kinase (p125^{FAK}) in invasive human tumors. *Cancer Res* **55**, 2752–2755.

[64] Tremblay L, Hauck W, Aprikian AG, Begin LR, Chapdelaine A, and Chevalier S (1996). Focal adhesion kinase (pp125^{FAK}) expression, activation and association with paxillin and p50^{CSK} in human metastatic prostate carcinoma. *Int J Cancer* **68**, 164–171.
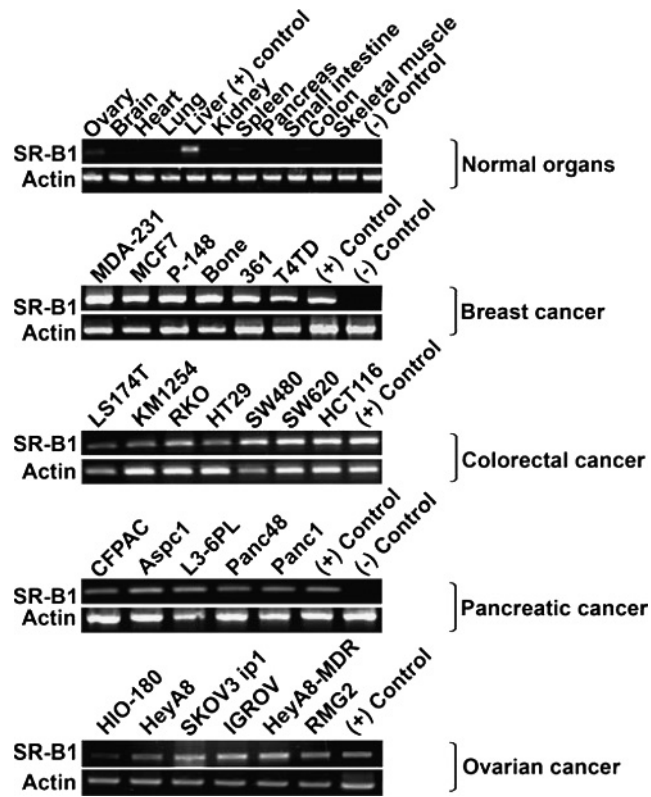
Figure W1. Expression of SR-B1 mRNA in different human organs and tumors using RT-PCR. Actin is used as a loading control.
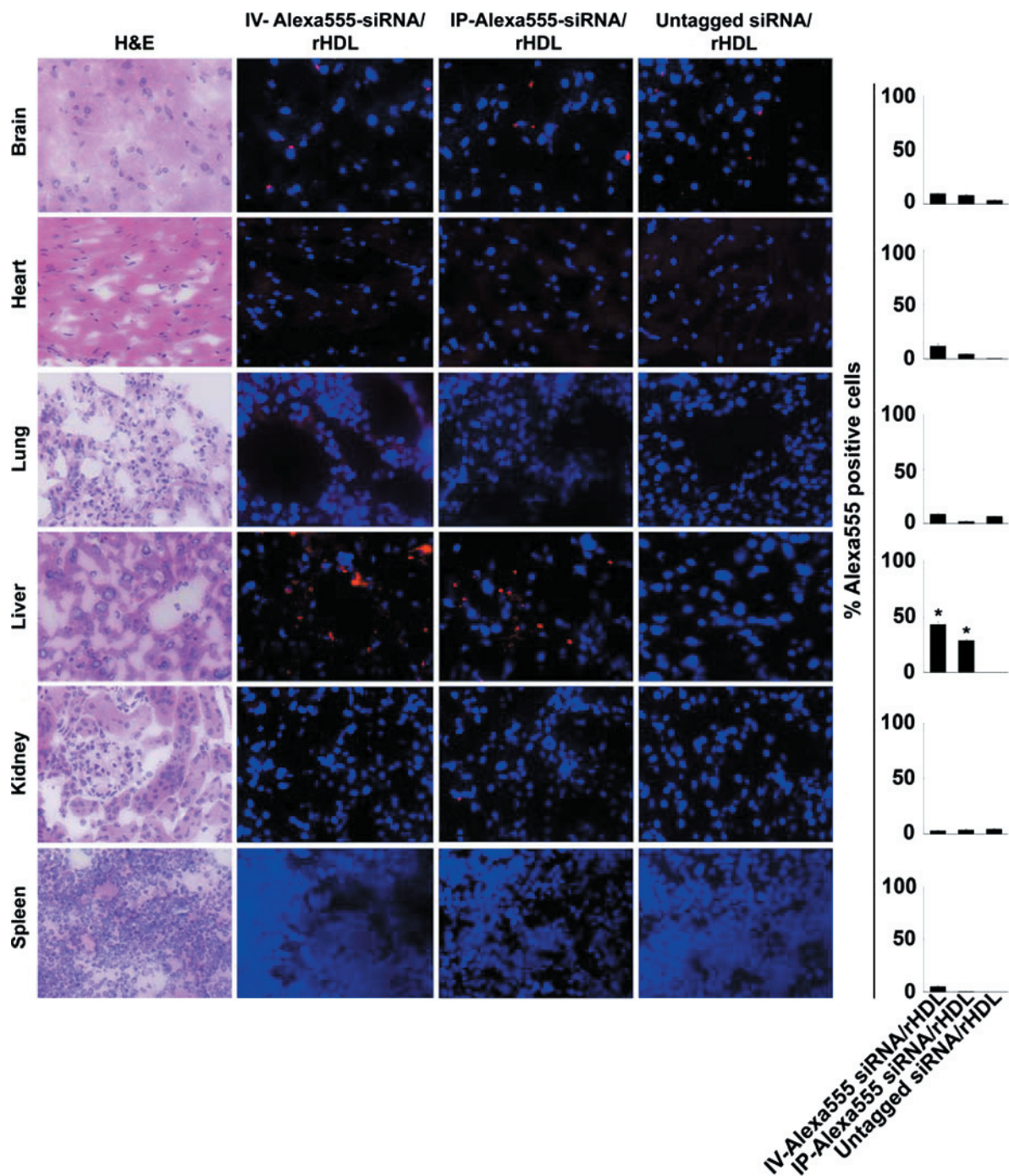
Figure W2. Distribution of systemic delivery of fluorescent-labeled siRNA/rHDL. Alexa555-labeled control siRNA/rHDL or untagged siRNA/rHDL was injected (IV or IP), and 48 hours later, organs were harvested. Fresh-frozen tissues were counterstained with Hoechst, and the level of fluorescent-labeled siRNA (red) was assessed with fluorescent microscopy. Average fluorescence uptake is represented by the graphs. *$P < .05$ compared with untagged siRNA/rHDL. H&E represents the organ morphology.
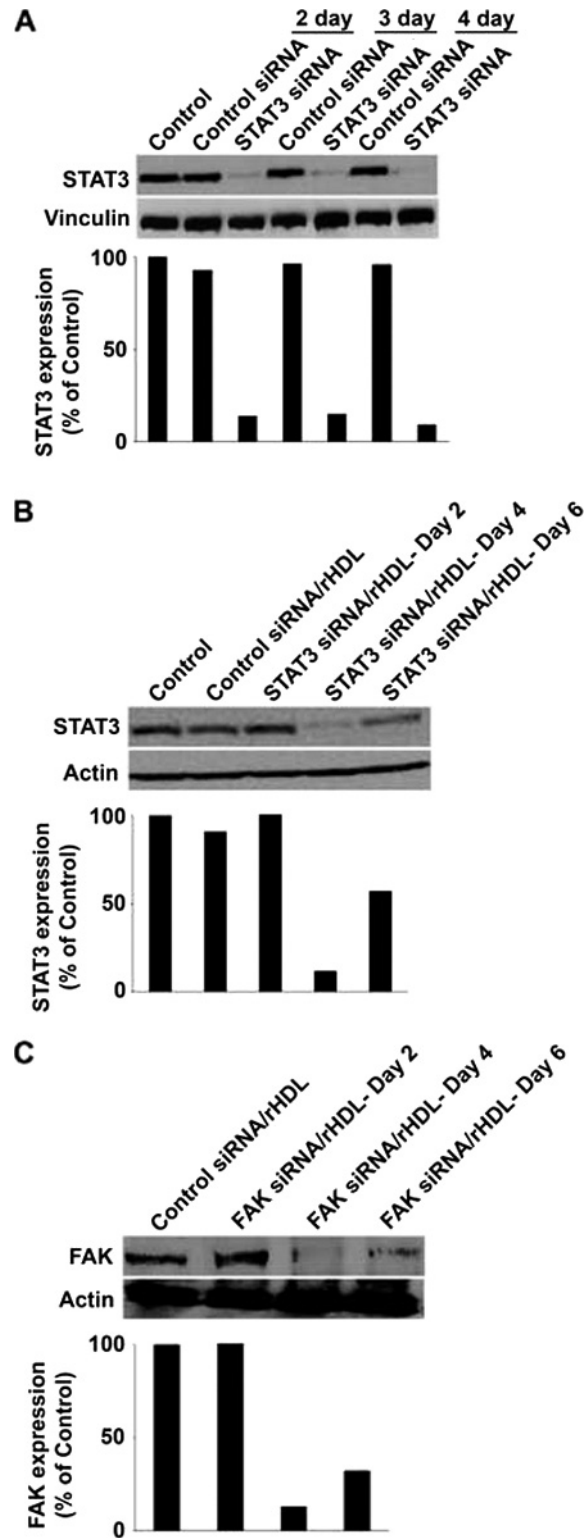
Figure W3. STAT3 and FAK silencing with siRNA/rHDL. (A) STAT3 siRNA treatment (*in vitro*) in SKOV3ip1 ovarian cancer cells. (B) STAT3 siRNA/rHDL. (C) FAK siRNA/rHDL was injected in mice bearing SKOV3ip1 ovarian tumors. Western blot analysis demonstrates relative protein expression. Graphs represent mean expression intensity measured with densitometry.
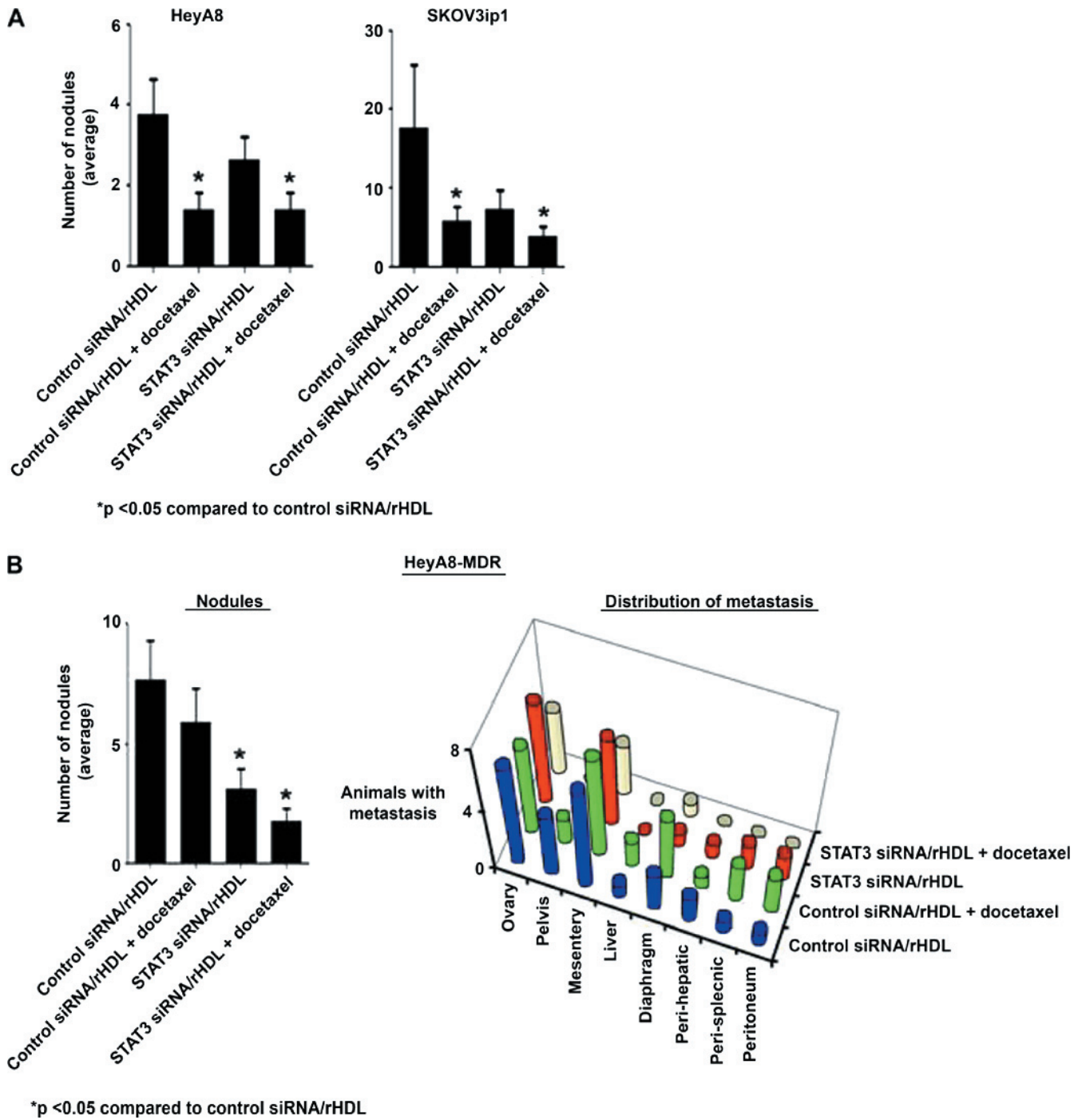
Figure W4. *In vivo* effect of STAT3 siRNA/rHDL with and without docetaxel therapy on tumor nodules in (A) HeyA8 and SKOV3 and (B) HeyA8-MDR ovarian cancer models. The average number of tumor nodules is presented as a bar graph. Error bars, SEM. Three-dimensional graph depicts the distribution of ovarian tumor metastasis in HeyA8-MDR (Taxol-resistant) ovarian cancer model.
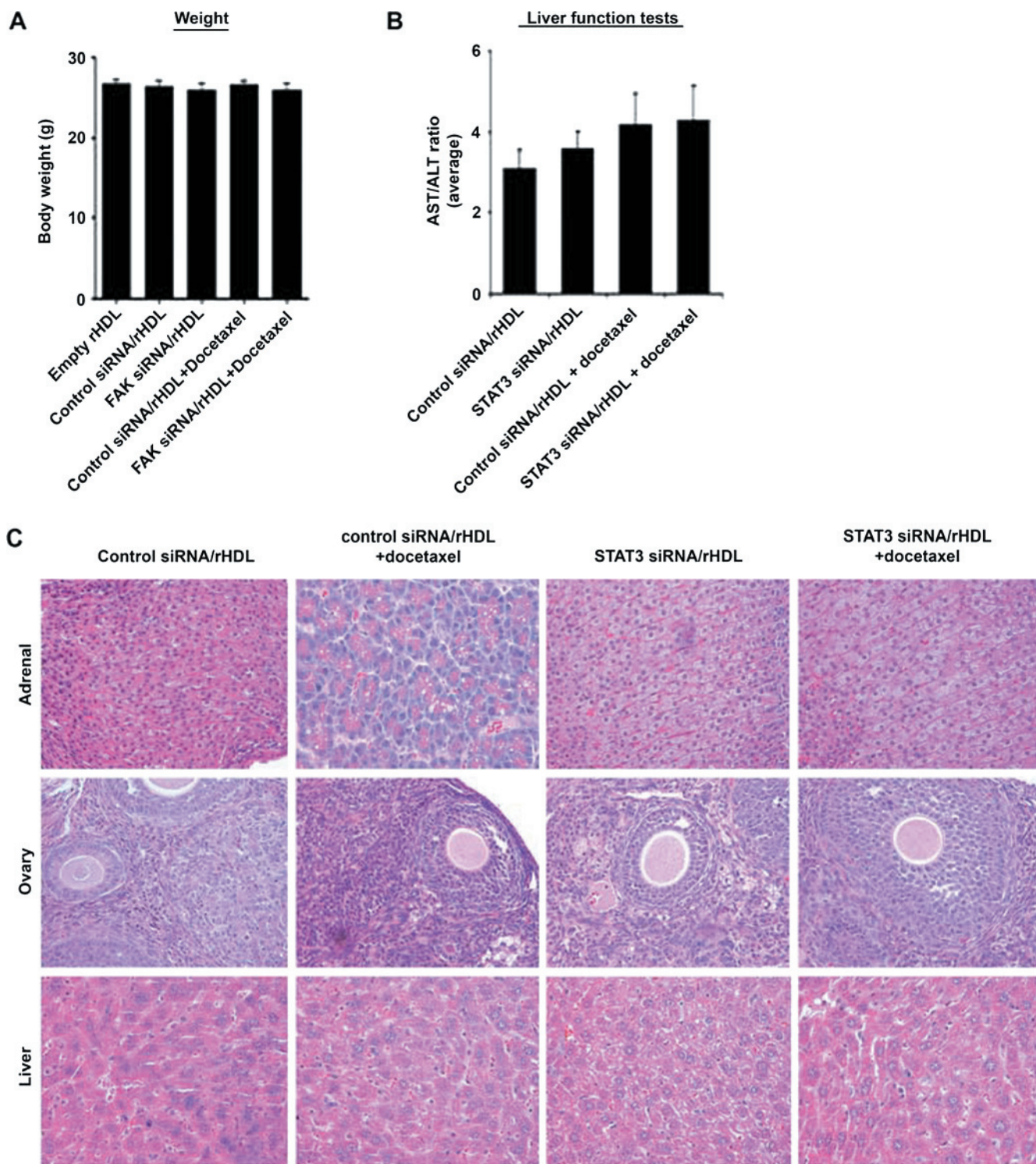
Figure W5. Safety of rHDL nanoparticles. (A) Body weights. (B) Liver function tests (LFTs) measured at the end of therapy experiment from all treatment groups are reported (for LFTs, AST and ALT ratio is presented). (C) Immunohistochemistry (IHC) performed on organs after a long-term therapy experiment. Representative images of IHC from each treatment group are presented.
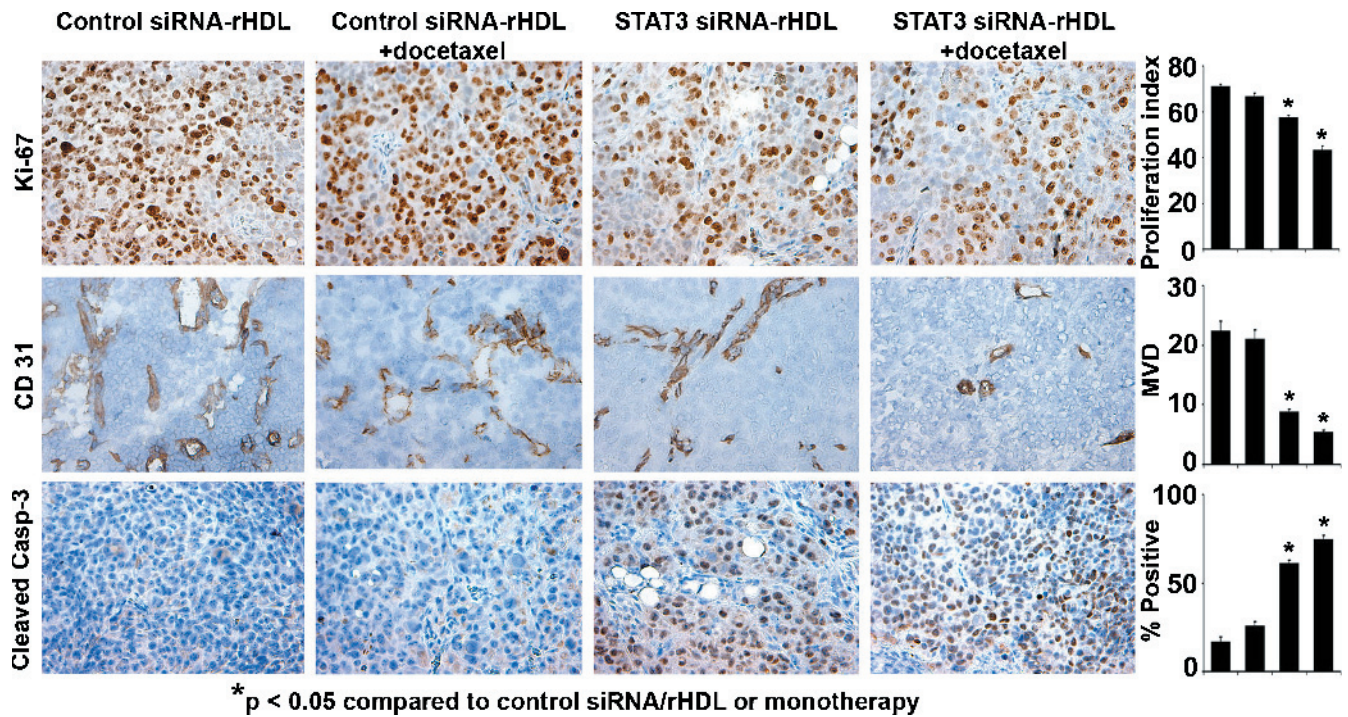
Figure W6. Effect of rHDL-incorporated STAT3 siRNA on tumor microenvironment. Tissues harvested after STAT3 siRNA/rHDL therapy from HeyA8-MDR ovarian cancer mouse model were subjected to immunohistochemistry for markers of proliferation (Ki-67), angiogenesis (CD 31), and apoptosis (cleaved caspase-3). For the analysis, five random fields per slide were examined with light microscopy and number of average number of microvessels (MVD) or the number of cells positive (Ki-67 and cleaved caspase-3) and nuclei are reported as average percent positive cells (200×). Error bars, SEM.

Table W1. Effect of Stat3 Silencing on Tumor Cell Apoptosis–Related Genes.

Gene	Fold Change	Gene	Fold Change
ALOX5	1.43	KITLG	0.66
ATF6	0.44	NFKBIZ	0.65
BAX	1.49	NQO1	0.55
BCL6	0.72	NRP1	0.67
BEX2	1.46	PLAUR	0.72
CAV1	0.75	PMAIP1	0.69
CD24	0.73	PMEPA1	0.71
CDCP1	0.73	PRKRA	0.68
CTGF	0.62	RASA1	0.68
CYR61	0.68	RTN1	1.37
DKK1	0.72	SFRP1	0.55
DUSP1	0.74	SGK1	0.68
ETS2	0.56	SPARC	0.7
FGF2	0.68	SPP1	0.77
FOS	0.72	STAT3	0.23
HMOX1	1.79	TCF3	0.71
IGFBP3	0.45	TNFRSF11B	0.61
IL-6	0.61	TNFSF10	0.7
IL-1B	0.55	XBP1	0.74

Gene expression changes after STAT3 silencing. Forty-eight hours after STAT3 silencing in ovarian cancer cells (SKOV3ip1), cDNA microarray analysis was performed. Average fold change in apoptosis-related genes is reported.